

# Fractional step code to model flow in a square cavity

Sashank Srinivasan

---

## Abstract

The goal of this project is to construct a 2-dimensional Navier-Stokes code to solve the generic lid driven cavity flow using the fractional step method, while solving a coupled Pressure Poisson equation using a SOR scheme. A cartesian grid composed of equally spaced grid points is used to discretize the governing equations using a second order central difference scheme with time stepping performed by an explicit euler scheme. The mesh layout used to implement the fractional step method is the collocated grid layout. The code written for the project is modular with different elements of the computational procedure clearly defined.

*Keywords:* Navier-Stokes equation, Pressure Poisson equation, lid driven cavity flow, finite difference, Fractional step method, collocated grid

---

## 1 Introduction

All fluid flow, regardless of the flow regime or the type of fluid, is governed by the Cauchy momentum equations in combination with the mass balance equation (1). When the assumption of the fluid being Newtonian is made, the Cauchy momentum equations reduce to the Navier-Stokes equations (2). These are a set of coupled partial differential equations that govern the spatial and temporal evolution of fluid velocities and pressure in a given domain. They are essentially mathematical representations of conservation of momentum in the x,y and z coordinates. When constant fluid temperature is assumed , the Navier-Stokes equations along with the continuity equation form a closed set of equations to solve for the velocities in the three directions and the pressure in the domain.

$$\frac{\partial \rho}{\partial t} + \nabla \cdot (\rho \vec{U}) = 0 \quad (1)$$

$$\rho \frac{D\vec{U}}{Dt} = -\nabla P + \mu \nabla^2 \vec{U} + \rho \vec{g} \quad (2)$$

### 1.1 Lid driven cavity flow

The fluid flow problem considered in this project is the 2-dimensional lid driven cavity flow. The domain is a 2-dimensional box with the right, left and bottom surfaces of the box fixed in position. The fluid is not allowed to penetrate through these three stationary surfaces. The top surface (lid) is moved at a finite velocity which imparts a velocity to the fluid in the region closest to the lid. The mechanism by which the velocity is imparted is the no-slip condition at the top surface. With the passage of time, the fluid in the entire cavity

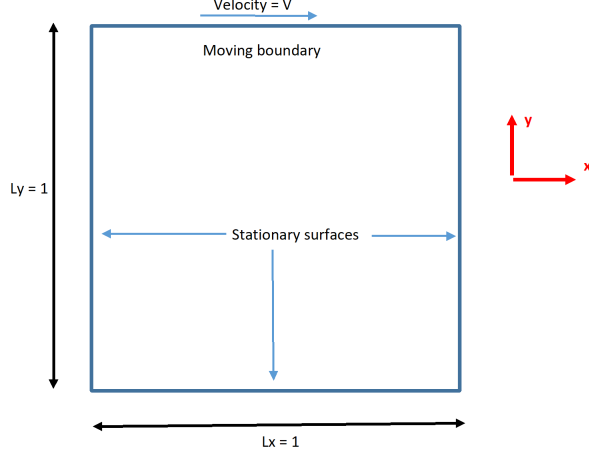


Figure 1: Domain of the flow considered

starts to flow within the cavity, resembling circulation. Hence this type of flow is termed recirculating flow.

The domain considered is a 1 by 1 box and the velocity  $V_{boundary}$  imparted by the top surface is assumed to also be 1. The fluid is assumed to be incompressible with a density  $\rho = 1$ . The value of the viscosity  $\mu$  of the fluid is governed by the Reynold's number  $Re_L$  considered

$$Re_L = \frac{\rho V_{boundary} L}{\mu} \quad (3)$$

## 1.2 Governing equations

The fluid is considered to be incompressible and Newtonian with a constant viscosity. All body forces including gravity are neglected. Due to these assumptions, the continuity and momentum conservation equations simplify to the form

$$\frac{\partial u}{\partial x} + \frac{\partial v}{\partial y} = 0 \quad (4)$$

$$\rho \left( \frac{\partial u}{\partial t} + u \frac{\partial u}{\partial x} + v \frac{\partial u}{\partial y} \right) = - \frac{\partial P}{\partial x} + \mu \left( \frac{\partial^2 u}{\partial x^2} + \frac{\partial^2 u}{\partial y^2} \right) \quad (5)$$

$$\rho \left( \frac{\partial v}{\partial t} + u \frac{\partial v}{\partial x} + v \frac{\partial v}{\partial y} \right) = - \frac{\partial P}{\partial y} + \mu \left( \frac{\partial^2 v}{\partial x^2} + \frac{\partial^2 v}{\partial y^2} \right) \quad (6)$$

The unknown variables solved for are the velocities  $u, v$  and the pressure  $P$ . All three quantities vary with both dimensions in space as well as time. The governing equations represent the physics of the problem. However, they are not solved in the exact form presented in this section. The fractional step method used in this project modifies the set of governing equations for computational purposes, and the details of the procedure is described in section 2.1.

## 2 Methods

This section describes the methodologies used to solve the governing equations. This includes the modification of the governing equations by the fractional step method, the finite difference formulation and code structure.

### 2.1 The Fractional step method

The governing equations are solved using the fractional step method. In this methodology, the governing equations are recast using fractional velocities  $\hat{u}, \hat{v}$  that are governed by the following equations

$$\rho \left( \frac{\partial \hat{u}}{\partial t} + u \frac{\partial u}{\partial x} + v \frac{\partial u}{\partial y} \right) = \mu \left( \frac{\partial^2 u}{\partial x^2} + \frac{\partial^2 u}{\partial y^2} \right) \quad (7)$$

$$\rho \left( \frac{\partial \hat{v}}{\partial t} + u \frac{\partial v}{\partial x} + v \frac{\partial v}{\partial y} \right) = \mu \left( \frac{\partial^2 v}{\partial x^2} + \frac{\partial^2 v}{\partial y^2} \right) \quad (8)$$

The terms  $u, v$  are the physical velocities which are the quantities ultimately solved for. During the time stepping procedure, we have the choice of using the values of  $u, v$  from the previous time step or the current time step. This represents if the scheme is an explicit or implicit scheme. The current work employs an explicit scheme. The pressure distribution is solved using the so called Pressure Poisson equation. This equation is obtained by differentiating the continuity with respect to time and then substituting expressions for the time derivative of  $u, v$  from the momentum conservation equations. After some manipulation of terms, we end up with the pressure Poisson equation given by

$$\frac{\partial^2 P}{\partial x^2} + \frac{\partial^2 P}{\partial y^2} = \frac{\partial \hat{u}}{\partial x} + \frac{\partial \hat{v}}{\partial y} \quad (9)$$

### 2.2 Boundary Conditions

The boundary conditions employed for the velocities are determined by the physics of the problem. All four boundaries do not allow any fluid to penetrate that particular surface. Hence we require that

$$\vec{U} \cdot \vec{n} = 0 \quad (10)$$

where  $\vec{n}$  represents the direction normal to the surface. All four boundaries also obey the no slip boundary condition. Hence we have at the left and right surfaces:  $v = 0$  and at the bottom boundary  $u = 0$ . On the top surface, we require that the velocity at the boundary be equal to velocity of the moving lid. Hence we have at  $y = 1$ ,

$$u = V_{boundary}, v = 0 \quad (11)$$

The pressure boundary condition has the following structure

$$\frac{\partial P}{\partial n} = 0 \quad (12)$$

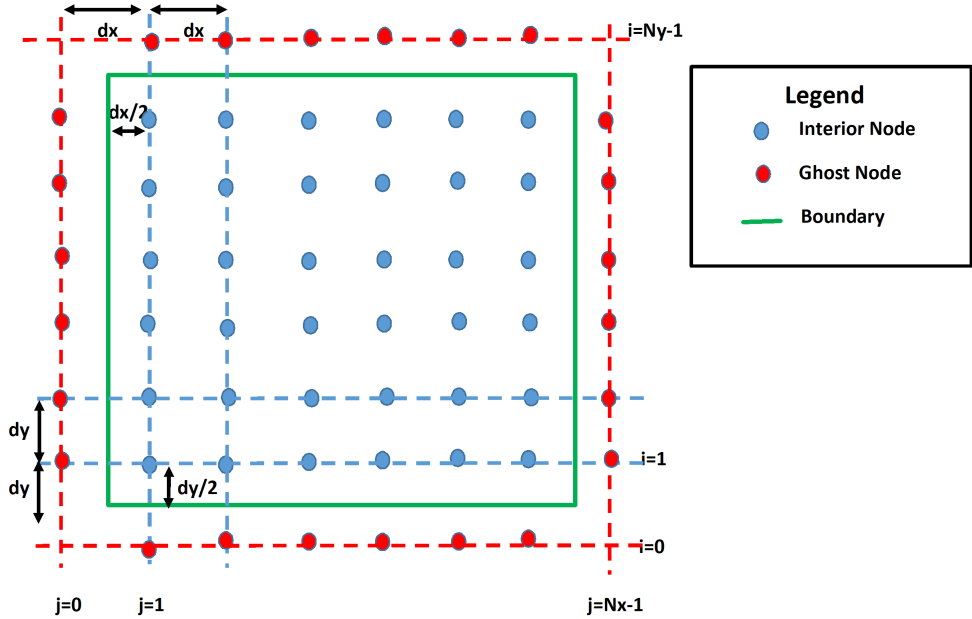


Figure 2: Notation used for naming nodes

Unlike the velocity boundary conditions, this applies to all boundaries. Also, the pressure boundary condition does not come from physical considerations, but rather to avoid a split pressure field that is disconnected from the boundary.

The exact way in which these boundary condition are implemented is given in section 2.6.

### 2.3 Notation of nodes

The notation used to refer to nodes is depicted in figure 2. The values of  $i, j$  run from  $i = 0$  to  $N_y + 1$  and  $j = 0$  to  $N_x + 1$ , where  $N_x = 40, N_y = 40$  which brings the total node count to 42 in each direction. Note that this is c++ notation. The nodes where  $i = 0$  or  $i = N_y + 1$  and  $j = 0$  or  $j = N_x + 1$  represent ghost nodes which are outside the domain.

The algorithm implemented is a **collocated grid**. Hence the velocities, fractional velocities and Pressure are calculated at node points  $(i, j)$  and are henceforth referred to as  $u_{i,j}, v_{i,j}, \hat{u}_{i,j}, \hat{v}_{i,j}, P_{i,j}$  respectively.

### 2.4 Finite difference formulation

The equations solved are (7), (8) and (9), which govern the spatial distribution and temporal evolution of the fractional velocities  $\hat{u}, \hat{v}$  and pressure  $P$  respectively. The time discretization is explicit euler and the spatial discretizations are second order central differencing which involves a five point stencil. The discretized equations for  $\hat{u}$  and  $\hat{v}$  are thus,

$$\begin{aligned} \frac{\hat{u}_{i,j}^{n+1} - u_{i,j}^n}{\Delta t} &= -u_{i,j}^n \left( \frac{u_{i,j+1/2}^n - u_{i,j-1/2}^n}{\Delta x} \right) - v_{i,j}^n \left( \frac{u_{i+1/2,j}^n - u_{i-1/2,j}^n}{\Delta y} \right) \\ &\quad + \frac{\mu}{\rho} \left( \frac{u_{i,j+1}^n + u_{i,j-1}^n - 2u_{i,j}^n}{\Delta x^2} \right) + \frac{\mu}{\rho} \left( \frac{u_{i+1,j}^n + u_{i-1,j}^n - 2u_{i,j}^n}{\Delta y^2} \right) \end{aligned} \quad (13)$$

$$\begin{aligned} \frac{\hat{v}_{i,j}^{n+1} - v_{i,j}^n}{\Delta t} &= -u_{i,j}^n \left( \frac{v_{i,j+1/2}^n - v_{i,j-1/2}^n}{\Delta x} \right) - v_{i,j}^n \left( \frac{v_{i+1/2,j}^n - v_{i-1/2,j}^n}{\Delta y} \right) \\ &\quad + \frac{\mu}{\rho} \left( \frac{v_{i,j+1}^n + v_{i,j-1}^n - 2v_{i,j}^n}{\Delta x^2} \right) + \frac{\mu}{\rho} \left( \frac{v_{i+1,j}^n + v_{i-1,j}^n - 2v_{i,j}^n}{\Delta y^2} \right) \end{aligned} \quad (14)$$

The velocities at half points such as  $(i, j + 1/2)$  or  $(i - 1/2, j)$  represent velocities at the cell faces rather than the nodes. These are not solved for directly but rather computed using the nodal velocities. The exact expression used depends on the type of flux scheme employed. In this project, the central flux scheme and the QUICK scheme are employed to understand if there is any difference in the simulation results or stability when the flux formulation is changed. The QUICK scheme is described in detail in section 2.5. The velocities at cell faces which are at the boundaries are computed using a simple central averaging.

The pressure Poisson equation is also discretized using a central differencing scheme, and the discretized equation looks like

$$P_{i,j} = \frac{1}{\left(\frac{1}{\Delta x^2} + \frac{1}{\Delta y^2}\right)} \left( \frac{1}{\Delta x^2}(P_{i,j+1} + P_{i,j-1}) + \frac{1}{\Delta y^2}(P_{i+1,j} + P_{i-1,j}) - (S_m)_{i,j} \right) \quad (15)$$

where  $(S_m)_{i,j}$  is the mass residual at node  $i, j$ , which is computed as

$$(S_m)_{i,j} = \frac{\hat{u}_{i,j+1/2}^{n+1} - \hat{u}_{i,j-1/2}^{n+1}}{\Delta x} + \frac{\hat{v}_{i+1/2,j}^{n+1} - \hat{v}_{i-1/2,j}^{n+1}}{\Delta y} \quad (16)$$

The fractional velocities at half nodes are computed as averages of the velocities at neighboring nodes

$$\begin{aligned} \hat{u}_{i,j-1/2} &= \frac{\hat{u}_{i,j} + \hat{u}_{i,j-1}}{2} \\ \hat{u}_{i,j+1/2} &= \frac{\hat{u}_{i,j} + \hat{u}_{i,j+1}}{2} \\ \hat{v}_{i-1/2,j} &= \frac{\hat{v}_{i,j} + \hat{v}_{i-1,j}}{2} \\ \hat{v}_{i+1/2,j} &= \frac{\hat{v}_{i,j} + \hat{v}_{i+1,j}}{2} \end{aligned} \quad (17)$$

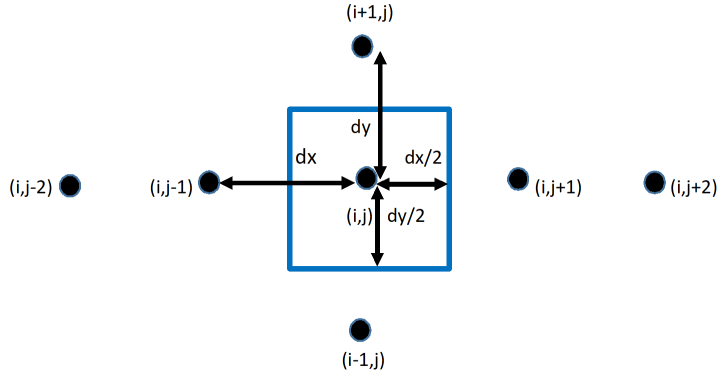


Figure 3: Distances between nodes and cell faces

## 2.5 The QUICK scheme for convection terms

The QUICK scheme is employed to approximate the values of velocities at cell faces. When compared to upwinding or central schemes, the QUICK scheme is slightly more complicated. The velocity values at cell faces are computed using quadratic fits which use values of 3 nodes surrounding the cell face in consideration. The exact nodes used in the fitting procedure depend on the direction of flow. To illustrate this, an example is used here.

Say we are interested in computing the term  $u_{i,j}^n \left( \frac{u_{i,j+1/2}^n - u_{i,j-1/2}^n}{\Delta x} \right)$  in equation (13). We need to use the QUICK scheme to find the values of  $u_{i,j-1/2}$  and  $u_{i,j+1/2}$ . According to the QUICK scheme the nodes used for the quadratic fit to approximate these values depend on the value of  $u_{i,j}$ . Use the notation in Figure 3 as a reference in the following discussion.

**Case 1:**  $u_{i,j} > 0$ . In this case the nodes used for the quadratic fit are  $(i, j - 2), (i, j - 1), (i, j)$  for approximating  $u_{i,j-1/2}$  and  $(i, j - 1), (i, j), (i, j + 1)$  for approximating  $u_{i,j+1/2}$ . Essentially, the QUICK scheme is using two "upwind" nodes and one "downwind" node. For example, in the case of  $u_{i,j-1/2}$ , the upwind nodes are  $(i, j - 2), (i, j - 1)$ . This is because of the direction of the flow in the x-direction which is given by the value of  $u_{i,j}$ , which in this case is positive. Once we know which nodes to use in the interpolation, the fit can be done as follows. Let's take the case where we want to approximate  $u_{i,j+1/2}$ . The quadratic fit will entail finding coefficients  $a, b, c$  such that

$$\begin{aligned}
 u_{i,j+1/2} &= a \\
 u_{i,j-1} &= a - b(3dx/2) + c(3dx/2)^2 \\
 u_{i,j} &= a - b(dx/2) + c(dx/2)^2 \\
 u_{i,j+1} &= a + b(dx/2) + c(dx/2)^2
 \end{aligned} \tag{18}$$

The fit for  $u_{i,j-1/2}$  can be performed in a similar manner. Once the coefficients are solved for, we end up with the following result

$$\begin{aligned}
u_{i,j-1/2} &= \frac{6}{8}u_{i,j-1} + \frac{3}{8}u_{i,j} - \frac{1}{8}u_{i,j-2} \\
u_{i,j+1/2} &= \frac{6}{8}u_{i,j} + \frac{3}{8}u_{i,j+1} - \frac{1}{8}u_{i,j-1}
\end{aligned} \tag{19}$$

**Case 2:**  $u_{i,j} < 0$ . This case represents flow in the opposite direction to case 1. The number of upwind and downwind nodes considered for the quadratic fit remain the same. But the upwind and downwind sense of directions are essentially reversed. Hence the nodes considered will change as follows

$$\begin{aligned}
u_{i,j-1/2} &: (i, j-1), (i, j), (i, j+1) \\
u_{i,j+1/2} &: (i, j), (i, j+1), (i, j+2)
\end{aligned}$$

and hence the fits will also change as

$$\begin{aligned}
u_{i,j-1/2} &= \frac{6}{8}u_{i,j} + \frac{3}{8}u_{i,j-1} - \frac{1}{8}u_{i,j+1} \\
u_{i,j+1/2} &= \frac{6}{8}u_{i,j+1} + \frac{3}{8}u_{i,j} - \frac{1}{8}u_{i,j+2}
\end{aligned}$$

The other terms in equations (13), (14) can be computed in a similar fashion, with care taken on using the correct nodes to approximate the cell face velocities based on the direction of the flow.

## 2.6 Discretization near the boundaries

The discretization near the boundaries needs to take into account the boundary conditions for the two velocities and Pressure. For the velocities, we have three choices: either the no penetration boundary condition, the no slip boundary or impart the velocity at which the lid is moving. In case of the no slip and the lid moving boundary, the ghost node velocities will be such that

$$\begin{aligned}
u_{boundary} &= \frac{u_{ghost} + u_{i,j}}{2} \\
v_{boundary} &= \frac{v_{ghost} + v_{i,j}}{2}
\end{aligned}$$

where  $(i, j)$  is the node closest the boundary and in consideration. For the no penetration, we will have the ghost node velocity equal to the velocity in the interior node.

**The no slip boundary condition:** essentially means that the velocity parallel to the surface is zero. Hence this will turn into setting either  $u_{boundary} = 0$  or  $v_{boundary}$  in the above equations at the boundary at all time steps.

**The no penetration of boundaries:** This means that the velocity in the direction parallel to the surface is zero. So this would again mean that either  $u_{boundary} = 0$  or  $v_{boundary}$  at the boundary. Hence the implementation of this boundary condition is the same as the previous case.

**At the lid:** We will have the  $u$  velocity at the boundary equal to velocity at which the boundary is moving and the  $v$  velocity will obey the no penetration boundary condition. These can be implemented in the same way as given above, either by setting  $u_{boundary}$  equal to the velocity of the moving lid, and by following the methodology for the no penetration case.

Once the ghost node velocities are set, they can be used in the discretized equations. The pressure boundary condition is given by equation (12), which transforms into the following discretized equation

$$P_{ghost} = P_{i,j}$$

where  $(i, j)$  is the interior node closest to the ghost node. Also, the velocity boundary conditions need to be implemented in the pressure Poisson equation. The pressure Poisson equation, when discretized, has fractional velocities at the cell faces. When a node closest to the boundary is considered, this will mean that we will need a value for the fractional velocity at the boundary. This will turn out to be the actual velocity at the boundary. Hence we have

$$\hat{u}_{boundary} = u_{boundary}$$

$$\hat{v}_{boundary} = v_{boundary}$$

Since we know the exact value of  $u_{boundary}, v_{boundary}$  at all surfaces, those values should be used.

## 2.7 Solution algorithm

The pressure Poisson equation is solved using the successive over-relaxation procedure. The SOR scheme is an iterative procedure where the values of pressure at each node  $(i, j)$  is guessed to be some value initially. The discretized pressure Poisson equation (15) is then solved at each node with values of pressure at neighboring nodes taken as the most recently calculated values in the iterative procedure. For the current Pressure Poisson equation at hand (9), when second order central differencing is used, the SOR scheme can be mathematically described as

$$P_{i,j} = P_{i,j}^{old} + \omega(P_{i,j} - P_{i,j}^{old}) \quad (20)$$

where  $P_{i,j}$  is the value of Pressure calculated node  $i, j$  in the current iteration and  $P_{i,j}^{old}$  is the pressure value at node  $ij$  in the previous iteration. For the SOR procedure,  $\omega > 1$

and in this case  $\omega$  was set to be equal to 1.4 for all simulations. The iterative procedure is continued until a residual of  $R_P = 10^{-3}$  is attained, where  $R_P$  is

$$R_P = \left( \sum_{i,j} \left( \frac{(P_{i,j+1} + P_{i,j-1} - 2P_{i,j})}{\Delta x^2} + \frac{(P_{i+1,j} + P_{i-1,j} - 2P_{i,j})}{\Delta y^2} - (S_m)_{i,j} \right)^2 \right)^{0.5} \quad (21)$$

For the current project, three Reynold's numbers of 50, 100 and 400 were considered. . All simulations were run at time step values below the time step limit governed by the stability criterion namely,

$$\Delta t < \frac{1}{\frac{|u|}{\Delta x} + \frac{|v|}{\Delta y} + \frac{2\mu}{\Delta x^2} + \frac{2\mu}{\Delta y^2}} \quad (22)$$

The simulations were run either till a final time of  $t = 10$  or until convergence was achieved, whichever is the later. The convergence criterion to determine if steady state is attained was taken to be  $R < 10^{-5}$ , where  $R$  is the residual defined as

$$R = \frac{\left( \sum_{i,j} [(u_{i,j}^n - u_{i,j}^{n-1})^2 + (v_{i,j}^n - v_{i,j}^{n-1})^2] \right)^{0.5}}{(N_x - 2)(N_y - 2)} \quad (23)$$

## 3 Results

### 3.1 Results for various Reynolds numbers

Reynold's numbers of  $Re_L = 50, 100, 400$  were used to create the plots shown in this section. The time step value used for all cases was below the time step limit governed by equation (22). All cases were run until a final time of  $t = 10.0$ , by which all three Reynold's number cases had attained steady state. This is clear in the plot of residual time shown, where the residuals reach a value below  $R = 10^{-5}$ , which is the threshold to gauge if steady state has been achieved.

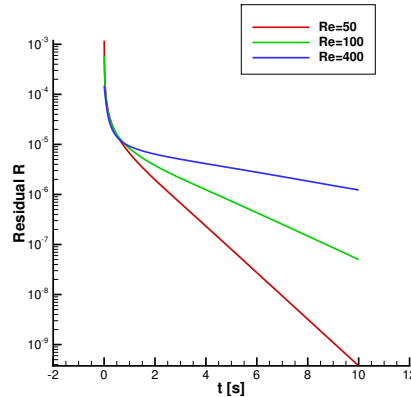


Figure 4: Residual vs time for different Reynold's numbers

### 3.1.1. Reynold's number = 50

From the plots of streamlines at various times, we can observe that the flow is very slightly symmetric about  $x = 0.55$ . This symmetry shifts towards  $x = 0.5$  as time increases. As we move in time, small recirculation zones develop at the two bottom corners, and are fully developed by time  $t = 10.0$ . The one on the right corner forms first, which is a common trend with all the three Reynold's numbers. The two zones are almost equal in size, which is in contrast to the other two cases. The pressure contours are always such that the maximum pressure is on the top right corner and minimum on the top left corner. This is in agreement with what is expected theoretically. The u velocity plots along the centerline show that the no slip boundary condition is obeyed always at the bottom and top boundaries. As we march in time the location of minimum u velocity moves downwards. The minimum u velocity also decreases as time increases. The v velocity curves show that the no-slip boundary condition is achieved, although less strictly compared to the u velocity. As time increases we see that the location of  $v = 0$  along the horizontal centerline remains more or less fixed at  $x \approx 0.55$ .

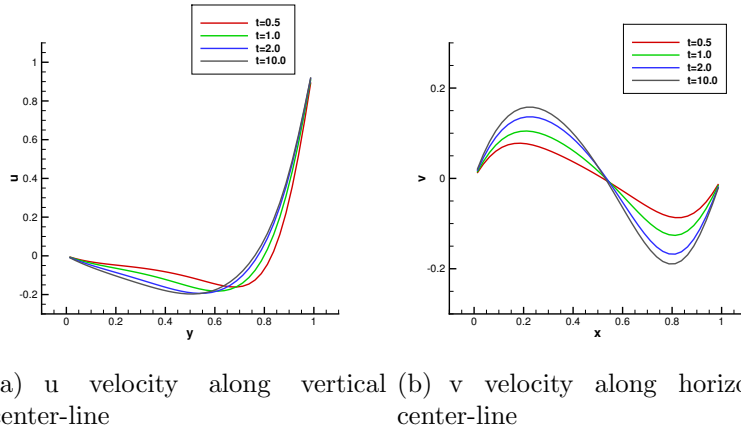
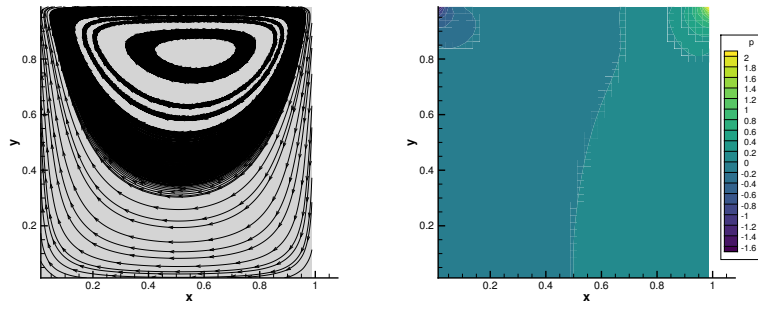
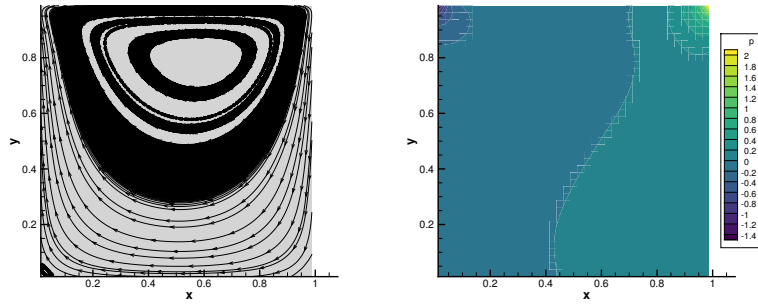


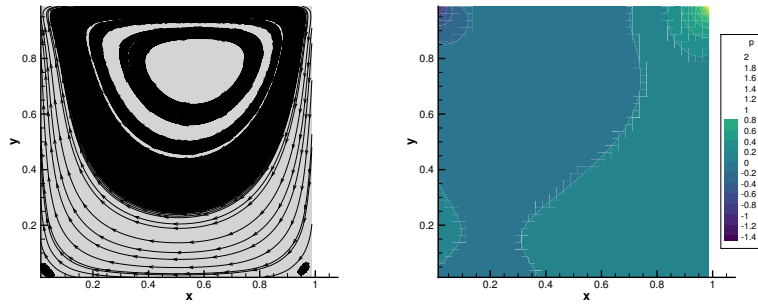
Figure 5: u and v velocities along horizontal and vertical center-lines at various times for Reynold's number=50



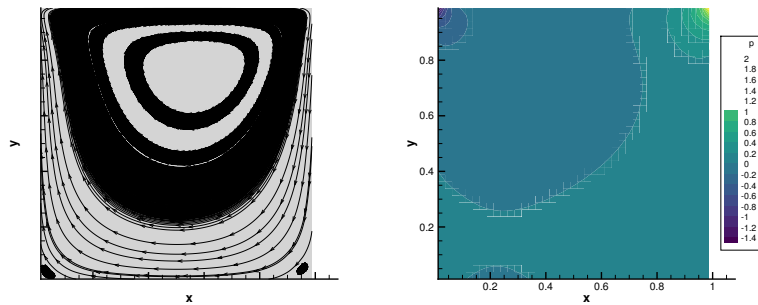
(a)  $t=0.5$



(b)  $t=1.0$



(c)  $t=2.0$



(d)  $t=10.0$

Figure 6: Streamlines and pressure contours at various times for Reynold's number=50

### 3.1.2. Reynold's number = 100

From the plots of streamlines at various times, we can observe that the flow is not symmetric, even during the initial times, which is unlike the previous Reynold's number. As time increases, the flow starts to shift towards the right. This effect is mild compared to the  $Re_L = 400$  case, but significant when compared to  $Re_L = 50$ . As we move in time, recirculation zones develop at the two bottom corners. These are more pronounced than the  $Re_L = 50$  case. The recirculation zone on the bottom right corner is slightly larger than the one on the left corner. The pressure contours are again always such that the maximum pressure is on the top right corner and minimum on the top left corner. The u velocity plots along the centerline show that the no slip boundary condition is obeyed always at the bottom and boundaries. The v velocity curves show that the no-slip boundary condition is obeyed to the same extent as the previous Reynold's number case. As time increases we see that the location of  $v = 0$  along the horizontal centerline changes very slightly towards the left of the domain.

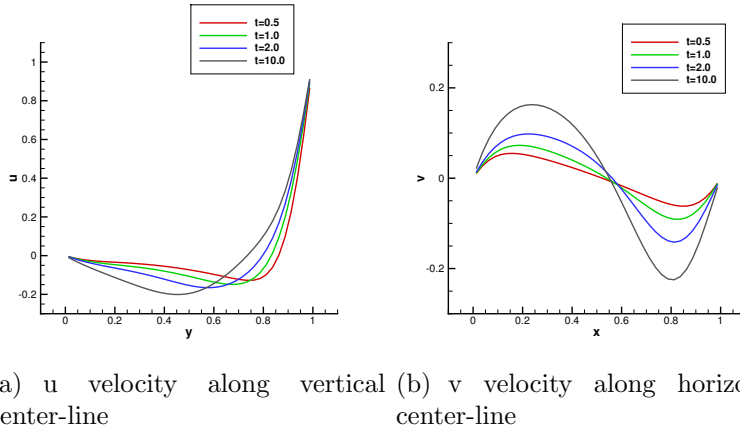
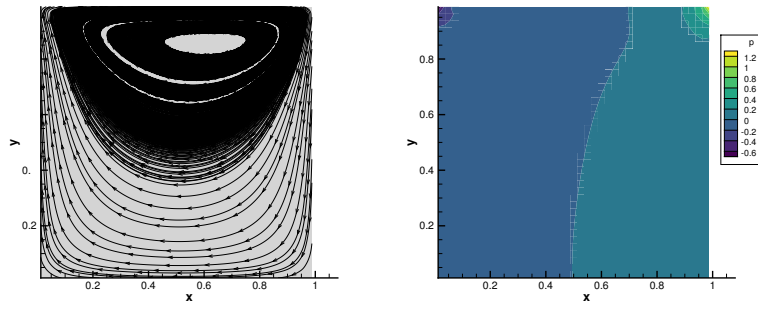
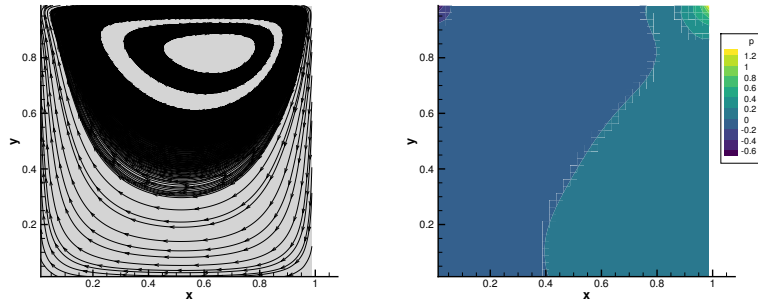


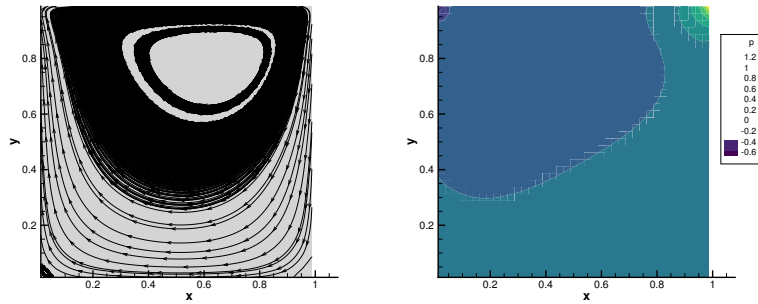
Figure 7: u and v velocities along horizontal and vertical center-lines at various times for Reynold's number=100



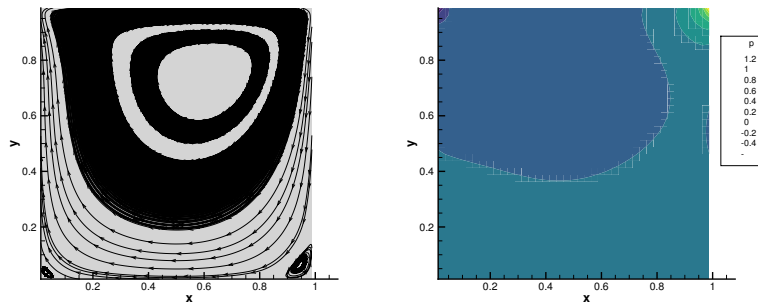
(a)  $t=0.5$



(b)  $t=1.0$



(c)  $t=2.0$



(d)  $t=10.0$

Figure 8: Streamlines and pressure contours at various times for Reynold's number=100

### 3.1.3. Reynold's number = 400

From the plots of streamlines at various times, we can observe there is no symmetry at all. The recirculation zone on the right corner is much more predominant. The pressure contours are again always such that the maximum pressure is on the top right corner and minimum on the top left corner. However, the changes in the contour as time increases are much more drastic when compared to the previous cases. The u velocity plots along the centerline show that the no slip boundary condition is obeyed always at the bottom and top boundaries. The time evolution of the profiles look different from before. Until time  $t = 2.0$ , there is not much change in the shape of the profiles. At time  $t = 10$ , the profile changes drastically, and is also drastically different when compared to  $Re_L = 50$  and  $Re_L = 100$  cases at the same time value. The v velocity curves also show a similar trend in that the profiles do not change drastically till  $t = 2.0$ , while at  $t = 10.0$ , the profile is changed significantly. The no-slip boundary condition is obeyed at both the left and right boundaries. The minimum and maximum v velocities are much larger in magnitude when compared to the previous two cases.

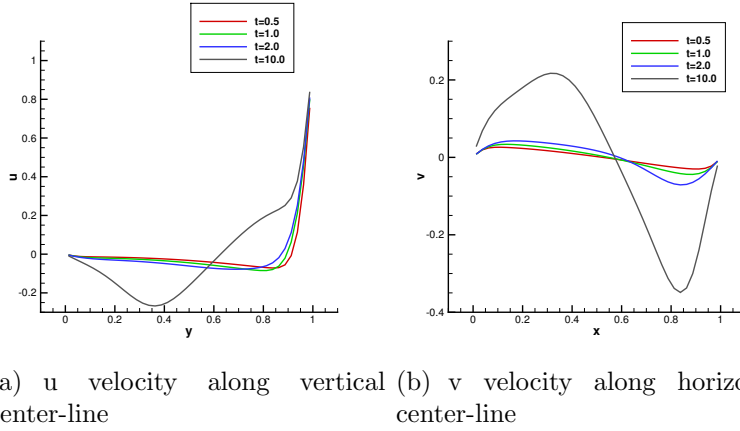
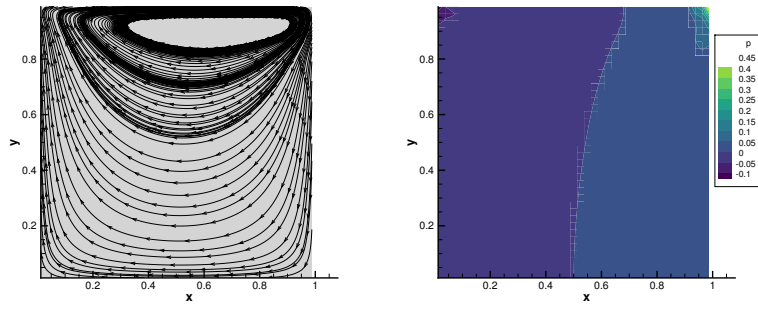
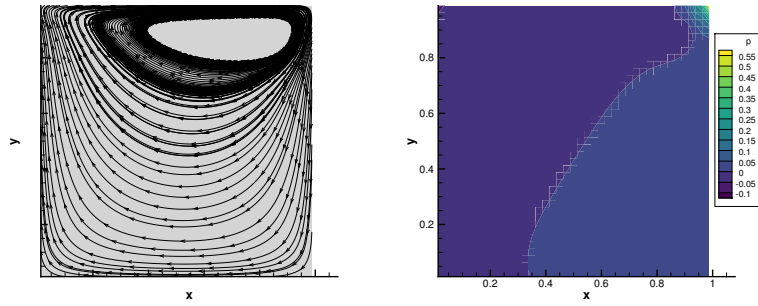


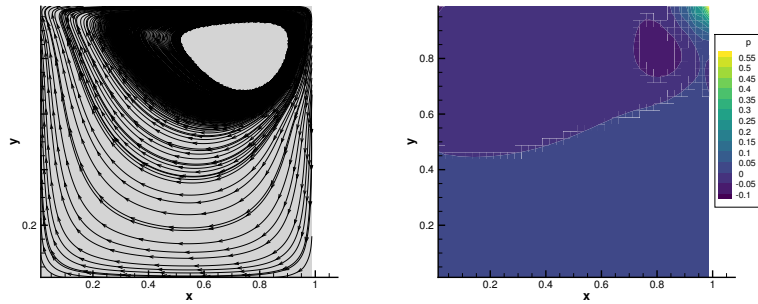
Figure 9: u and v velocities along horizontal and vertical center-lines at various times for Reynold's number=400



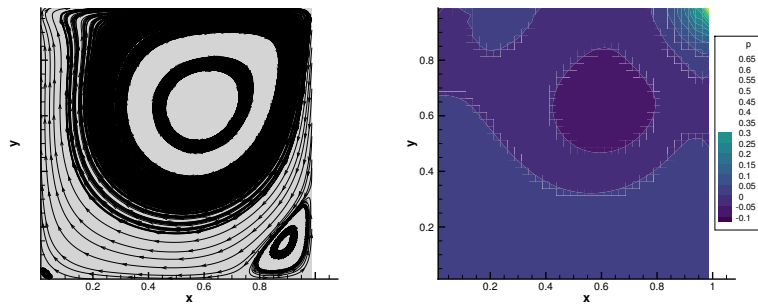
(a)  $t=0.5$



(b)  $t=1.0$



(c)  $t=2.0$



(d)  $t=10.0$

Figure 10: Streamlines and pressure contours at various times for Reynold's number=400

### 3.2 Comparison to Literature

To assess the accuracy of the code built, results from published works were used to see if the current code is able to generate similar if not the same result. To this end, a couple of highly cited works were chosen.

The first comparison made is results published by Ghia, Ghia, and Shin [1]. Results for  $Re_L = 100, 400$  are published in this work. A side by side comparison to results generated by the current code shows good agreement, as can be observed in Figure 11. At both Reynold's numbers, the comparison is very good.

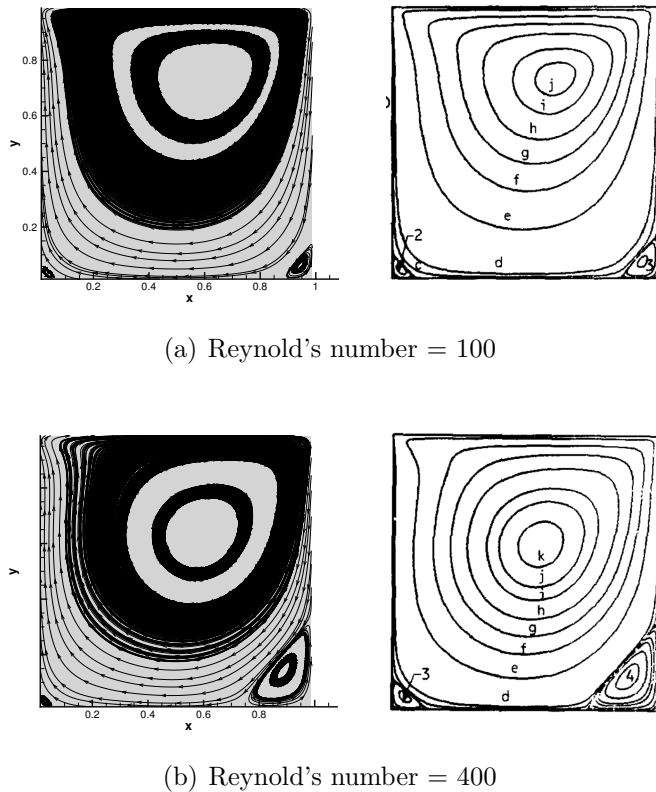
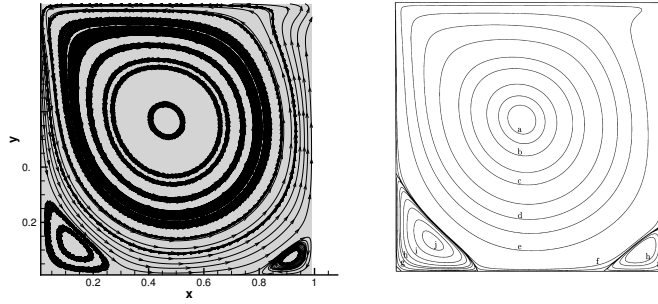


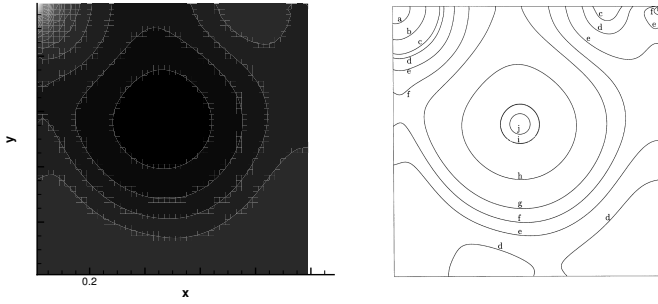
Figure 11: Comparison of streamlines at different Reynold's to results from [1] (right figures)

The second comparison made is to results published by Botella and Peyret [2], who use spectral methods to simulate the same problem. They use a Reynold's number of 1000 and show plots of streamline and pressure contours. When the same case is simulated using the current code, a very good agreement of results is observed. The comparisons are shown in Figure 12. The streamline comparison shows excellent agreement. The recirculation zones are captured well, though the current results show the zones to be slightly smaller in size. The pressure contour comparison shows very minimal difference (mainly at the top left corner). However considering the fact that Botella and Peyret used a high order scheme with a much larger grid, the current code fares very well.

The final comparison made is using results from a study by Bruneau and Saad [3]. They publish results using different Reynold's numbers for the same problem analyzed here. The results published for  $Re_L = 5000$  are chosen for comparison because three recirculation zones



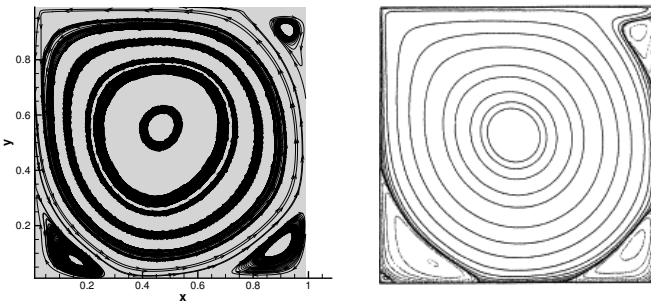
(a) streamlines comparison



(b) pressure contours comparison

Figure 12: Comparison of results at Reynold's number=1000 (left figures) to [2]

are predicted, rather than two which has been the case with all the results so far. The steady state solutions of  $Re_L = 5000$  shows good comparison again, as can be observed in Figure 13. All three recirculation zones are captured by the current code. However, the current predictions suffer from the same drawback that the zones predicted are of a smaller size.



(a) streamlines comparison

Figure 13: Comparison of results at Reynold's number=5000 (left figure) to [3]

### 3.3 Overall observations

The problem statement is given in terms of non-dimensional numbers, and the fluid properties are also not specified. Thus the domain dimensions, values of  $\rho, \mu, V_{boundary}$  can be chosen arbitrarily (provided they give the required Reynold's numbers). The results presented till now used values of  $L_x = 1, L_y = 1, \rho = 1, V_{boundary} = 1$  and  $Re_L = 50, 100, 400$ . The value of  $\mu$  was computed based on the Reynold's number. Instead, if the fluid properties were considered to be that of air namely  $\rho = 1.225 \text{ kg/m}^3, \mu = 1.81 \times 10^{-5}$  and the domain lengths retained as 1, we would be computing  $V_{boundary}$  based on the Reynold's number. If these computations are run, the time step limit was found to be smaller and also the pressure Poisson equation required a larger number of iterations to converge. Further, if a smaller domain was considered, say  $L_x = 10^{-2}, L_y = 10^{-2}$ , the time step limit reduced drastically and the pressure Poisson equation did not converge if the convergence criterion was set to  $R_P = 10^{-3}$ . This was because the pressure values computed were  $\mathcal{O}(10^{-6})$ . Compared to pressure values of  $\mathcal{O}(1)$  when the original simulations were run, these new pressures are extremely small. Hence a mass residual of  $10^{-3}$  was extremely difficult to achieve in some runs, while in other cases, the iterative procedure plateaued at a residual value in the region  $R_P = 5 \times 10^{-3}$ .

### 3.4 Comparison of QUICK scheme with upwind fluxes

The current code uses QUICK scheme convection fluxes at interior cell faces and central fluxes on cell faces at the boundaries. Instead, one could perform the computations using central fluxes throughout the domain. A comparison to one such computation is presented here. The case of Reynold's number=50 is chosen, and results at steady state are compared. The streamlines plots and pressure contours look almost identical, as can be observed in Figure 15. No difference was observed in the time step limitation also. This can be seen in Figure 14.

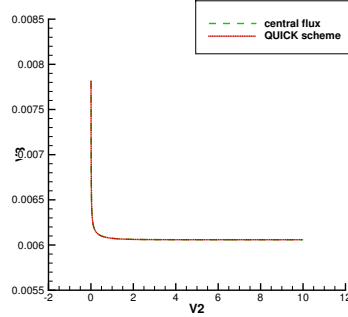
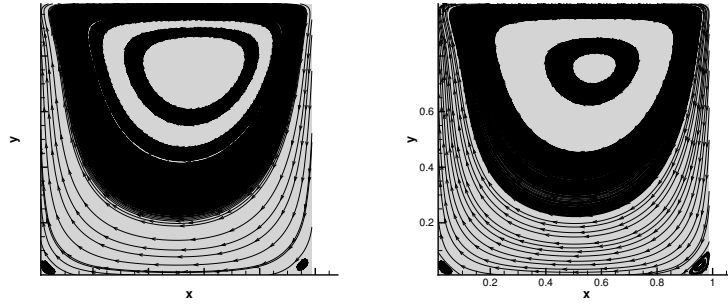


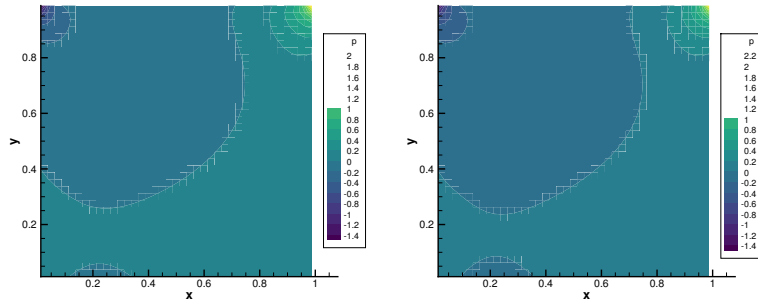
Figure 14: Comparison of time step limitation at Reynold's number=50 obtained using QUICK scheme fluxes and central fluxes (left figure show QUICK)

## 4 Conclusion

A fractional step code which solved for the flow field in a lid driven cavity flow was successfully built. The domain considered was of size  $1 \times 1$ , with 40 interior grid points



(a) streamlines comparison



(b) Pressure contours comparison

Figure 15: Comparison of results at Reynold's number=50 obtained using QUICK scheme fluxes and central fluxes (left figures show QUICK)

considered. Three different Reynold's numbers values were analyzed using constant density and Velocity boundary conditions, with the value of viscosity changed. The QUICK scheme was used to evaluate convection fluxes, and results obtained were compared to those obtained using central difference fluxes. Explicit time marching was used with the time step value smaller than the stability criterion. All simulations were until time  $t = 10.0$ , by when steady state was achieved. Results were compared to literature and also to those generated using central convection fluxes.

## References

- [1] U. Ghia, K. N. Ghia, C. Shin, High-Re solutions for incompressible flow using the Navier-Stokes equations and a multigrid method, *Journal of computational physics* 48 (3) (1982) 387–411.
- [2] O. Botella, R. Peyret, Benchmark spectral results on the lid-driven cavity flow, *Computers & Fluids* 27 (4) (1998) 421–433.
- [3] C.-H. Bruneau, M. Saad, The 2D lid-driven cavity problem revisited, *Computers & Fluids* 35 (3) (2006) 326–348.